Psychological Medicine (2017), **47**, 2689–2707. © Cambridge University Press 2017
doi:10.1017/S0033291717001210

ORIGINAL ARTICLE

Patterns of white matter microstructure in individuals at ultra-high-risk for psychosis: associations to level of functioning and clinical symptoms

K. Krakauer[1,2,3]*, B. H. Ebdrup[2,4], B. Y. Glenthøj[2,4], J. M. Raghava[2,3,4], D. Nordholm[1,2], L. Randers[1,2], E. Rostrup[3] and M. Nordentoft[1,2]

[1] *Mental Health Centre Copenhagen, Copenhagen University Hospital, DK-2900 Hellerup, Denmark*
[2] *Centre for Clinical Intervention and Neuropsychiatric Schizophrenia Research, CINS, DK-2600 Glostrup, Denmark*
[3] *Functional Imaging Unit, Clinical Physiology, Nuclear Medicine and PET, Copenhagen University Hospital Rigshospitalet, DK-2600 Glostrup, Denmark*
[4] *Centre for Neuropsychiatric Schizophrenia Research (CNSR), Mental Health Centre Glostrup, Copenhagen University Hospital, DK-2600 Glostrup, Denmark*

Background. Individuals at ultra-high-risk (UHR) for psychosis present with emerging symptoms and decline in functioning. Previous univariate analyses have indicated widespread white matter (WM) aberrations in multiple brain regions in UHR individuals and patients with schizophrenia. Using multivariate statistics, we investigated whole brain WM microstructure and associations between WM, clinical symptoms, and level of functioning in UHR individuals.

Methods. Forty-five UHR individuals and 45 matched healthy controls (HCs) underwent magnetic resonance diffusion tensor imaging (DTI) at 3 Tesla. UHR individuals were assessed with the Comprehensive Assessment of At-Risk Mental States, Scale for the Assessment of Negative Symptoms, and Social and Occupational Functioning Assessment Scale. Partial least-squares correlation analysis (PLSC) was used as statistical method.

Results. PLSC group comparisons revealed one significant latent variable (LV) accounting for 52% of the cross-block covariance. This LV indicated a pattern of lower fractional anisotropy (FA), axial diffusivity (AD), and mode of anisotropy (MO) concomitant with higher radial diffusivity (RD) in widespread brain regions in UHR individuals compared with HCs. Within UHR individuals, PLSC revealed five significant LVs associated with symptoms and level of functioning. The first LV accounted for 31% of the cross-block covariance and indicated a pattern where higher symptom score and lower level of functioning correlated to lower FA, AD, MO, and higher RD.

Conclusions. UHR individuals demonstrate complex brain patterns of WM abnormalities. Despite the subtle psychopathology of UHR individuals, aberrations in WM appear associated with positive and negative symptoms as well as level of functioning.

Received 23 November 2016; Revised 7 March 2017; Accepted 6 April 2017; First published online 3 May 2017

Key words: Diffusion tensor imaging, level of functioning, Partial Least Squares correlation analysis, psychopathology, ultra high-risk for psychosis.

Introduction

Ultra-high-risk (UHR) individuals refer to a group of individuals predominantly characterized by attenuated psychotic symptoms and marked reductions in level of functioning (Yung *et al.* 2003, 2005), but negative symptoms are also frequently reported (Meyer *et al.* 2014; Schlosser *et al.* 2015).

Cerebral white matter (WM) microstructure can be examined *in vivo* by diffusion tensor imaging (DTI), which is a magnetic resonance imaging (MRI) technique. From DTI data various tensor invariants can be obtained: fractional anisotropy (FA) and mean diffusivity (MD) reflecting the degree of directionality and average magnitude of molecular displacement by diffusion, and axial diffusivity (AD) and radial diffusivity (RD) reflecting diffusion parallel and perpendicular to the preferred direction of diffusion (Basser & Pierpaoli, 2011). Mode of anisotropy (MO) reflects the degree to which anisotropy is planar (due to e.g. crossing fibers) or linear (as in a single fiber population

* Address for correspondence: K. Krakauer, M.D., Research Unit, Mental Health Centre Copenhagen, Gentofte Hospital, Kildegårdsvej 28, Opgang 15, 4. sal, 2900 Hellerup, Denmark.
(Email: kristine.krakauer@regionh.dk)

orientation) (Ennis & Kindlmann, 2006; Kindlmann *et al.* 2007; Wigand *et al.* 2015).

DTI has been increasingly applied in studies of patients with first episode psychosis (FEP) and schizophrenia (FES). These studies have indicated widespread aberrations in WM microstructure mainly characterized by FA reductions in various regions such as in the corpus callosum (Cheung *et al.* 2008; Gasparotti *et al.* 2009; Perez-Iglesias *et al.* 2010), superior longitudinal fasciculus (Perez-Iglesias *et al.* 2010; Guo *et al.* 2012), inferior longitudinal fasciculus (Cheung *et al.* 2008; Perez-Iglesias *et al.* 2010; Ebdrup *et al.* 2016), internal capsule including the corticospinal tracts and the anterior and superior thalamic radiations (Cheung *et al.* 2008; Perez-Iglesias *et al.* 2010; Guo *et al.* 2012; Filippi *et al.* 2014; Ebdrup *et al.* 2016), external capsule (Guo *et al.* 2012), and fronto-occipital fasciculus (Cheung *et al.* 2008).

Fewer studies have investigated WM structure in UHR individuals (Peters *et al.* 2008, 2009, 2010; Karlsgodt *et al.* 2009; Bloemen *et al.* 2010; Carletti *et al.* 2012; Pettersson-Yeo *et al.* 2013; Epstein *et al.* 2014; Mittal *et al.* 2014; von Hohenberg *et al.* 2014; Bernard *et al.* 2015; Katagiri *et al.* 2015; Schmidt *et al.* 2015; Cooper *et al.* 2016; Rigucci *et al.* 2016; Wang *et al.* 2016). Similar to findings in schizophrenia patients most of the studies find that UHR individuals have widespread regional FA reductions (Karlsgodt *et al.* 2009; Peters *et al.* 2009; Bloemen *et al.* 2010; Carletti *et al.* 2012; Epstein *et al.* 2014; Bernard *et al.* 2015; Katagiri *et al.* 2015; Cooper *et al.* 2016; Rigucci *et al.* 2016; Wang *et al.* 2016), although a few studies find no aberrations in FA (Peters *et al.* 2008, 2010; Mittal *et al.* 2014; von Hohenberg *et al.* 2014) or even an increase in FA (Schmidt *et al.* 2015) in UHR individuals compared with healthy controls (HCs). Reduced FA in the superior longitudinal fasciculus appears to be the most consistent finding in UHR studies (Karlsgodt *et al.* 2009; Bloemen *et al.* 2010; Carletti *et al.* 2012; von Hohenberg *et al.* 2014; Rigucci *et al.* 2016; Wang *et al.* 2016)

Currently it is unclear to what extent WM aberrations (if present) are associated with clinical symptoms and/or level of functioning in UHR individuals. Several studies have found a negative correlation between FA and severity of positive symptoms in UHR individuals and individuals experiencing subthreshold psychotic symptoms (Bloemen *et al.* 2010; Cooper *et al.* 2016; DeRosse *et al.* 2016; Wang *et al.* 2016); however, one study found the inverse correlation in some of the same areas (Schmidt *et al.* 2015). Moreover, lower FA at baseline has been found to predict deterioration in level of functioning at follow-up (Karlsgodt *et al.* 2009) and a longitudinal increase in FA has been correlated to an improvement in severity of positive symptoms in UHR individuals (Katagiri *et al.* 2015). In patients with schizophrenia findings are heterogeneous with findings of FA being both negatively and positively correlated to severity of positive (Hubl *et al.* 2004; Seok *et al.* 2007; Shergill *et al.* 2007; Skelly *et al.* 2008; Szeszko *et al.* 2008; Whitford *et al.* 2010; Catani *et al.* 2011; Cheung *et al.* 2011; Choi *et al.* 2011; Cui *et al.* 2011; Mulert & Scarr, 2012; Boos *et al.* 2013; Lee *et al.* 2013; Hatton *et al.* 2014; Caprihan *et al.* 2015; Ohtani *et al.* 2015; Ebdrup *et al.* 2016; Seitz *et al.* 2016; Zhang *et al.* 2016) and negative (Wolkin *et al.* 2003; Shin *et al.* 2006; Skelly *et al.* 2008; Szeszko *et al.* 2008; Lee *et al.* 2013; Asami *et al.* 2014; Ohtani *et al.* 2015; Sun *et al.* 2015; Zeng *et al.* 2016) symptoms.

Previous UHR studies in WM microstructure have employed univariate analysis investigating each diffusion parameter separately. However, it is likely that the complex pathological phenomena altering the tissue microstructure will affect several diffusion parameters simultaneously. In the present study, we are extending previous findings by doing joint analysis of diffusion parameters using multivariate analysis, which might provide additional information than the widely used univariate analysis (Konukoglu *et al.* 2016). To our knowledge this is the first study to explore multivariate patterns of WM microstructural pathology in UHR individuals and associating the patterns to clinical symptoms and level of functioning.

The clinical challenge of recruitment of UHR individuals is reflected in generally small samples sizes, which further challenge the application of conventional statistical procedures. Moreover, DTI data provide multiple interrelated measures, which require careful attention to problems with multiple comparisons, especially when interpreting voxelwise whole brain analyses. Multivariate statistical analyses, such as the partial least-square correlation (PLSC) procedure, may be superior to conventional univariate statistics to handle small sample sizes and interrelated measures (McIntosh *et al.* 1996; Nestor *et al.* 2002; McIntosh & Lobaugh, 2004; Krishnan *et al.* 2011).

Hypothesis

We hypothesized different patterns of WM microstructure in UHR individuals compared with HCs, with UHR individuals showing a pattern of low FA, high RD, and unchanged or low AD. We also hypothesized that clinical symptoms and the level of functioning would be associated with patterns of WM microstructure within the UHR individuals.

We explored this using a multivariate approach since the complex phenomena of UHR is more likely associated to patterns of diffusion aberrations than to

https://doi.org/10.1017/S0033291717001210 Published online by Cambridge University Press

strongly localized effects (Konukoglu *et al.* 2016). We used bootstrap tests to visualize the most reliable spatial regions showing these WM patterns. However, interpretation of the spatial localization should be done with caution since the PLSC uses the entire set of voxels as a single multivariate representation. We therefore did additional univariate analysis exploring voxelwise group differences in each DTI parameter, and correlating each clinical measure to the DTI parameters separately. We also tried to quantify the PLSC findings using the spatial regions found by PLSC as regions of interest (ROIs) and compared mean values of DTI parameters in these regions.

Method

The study was conducted in accordance with the declaration of Helsinki and approved by the Regional Ethics Committee of the Capital Region, Denmark (H-D-2009-013). Participants signed informed consent.

Participants

As part of an UHR project at Mental Health Centre Copenhagen, UHR individuals aged 18–40 years were recruited between December 2008 and December 2014 from psychiatric in- and outpatient services in the Capital Region of Denmark. Individuals had to be help-seeking and fulfill criteria for one or more of the three UHR categories as assessed by the Comprehensive Assessment of At-Risk Mental States (CAARMS) (Yung *et al.* 2003, 2005): (1) attenuated psychotic symptoms (APS); (2) brief limited intermittent psychotic symptoms (BLIPS); (3) trait and state (schizotypal personality disorder or a history of psychosis in a first-degree relative) (TS). An additional inclusion criterion was a decline in functioning ($\geqslant$30% drop for at least one month), or sustained low functioning ($\leqslant$50 for at least a year) assessed with the Social and Occupational Functioning Assessment Scale (SOFAS) (Goldman *et al.* 1992; Hilsenroth *et al.* 2000).

Exclusion criteria were: organic brain disease, a diagnosis of a serious developmental disorder (e.g. Asperger's syndrome), IQ < 70 (as measured by the Wechsler Adult Intelligence Scale – Third Edition (WAIS-III)) (Wechsler, 1997), psychiatric symptoms explained by acute intoxication or a physical illness with psychotropic effect, past history of a psychotic episode of more than one week, current treatment with mood stabilisers or methylphenidate, antipsychotic medication exceeding a total lifetime dose of 50 mg haloperidol or equivalent antipsychotic medication (Andreasen *et al.* 2010), and pregnancy (tested with a urine HCG pregnancy test).

HCs were included between April 2009 and May 2014 as part of the *Pan European Collaboration Antipsychotic-Naive Studies* at Psychiatric Centre Glostrup. HCs had no first degree relatives with a psychotic disorder and underwent psychopathology assessments using the Schedules for Clinical Assessment in Neuropsychiatry Version 2.1 (Wing *et al.* 1990) to ensure that they had no current or previous psychiatric diagnoses including substance abuse or dependency. The HCs were matched to the UHR individuals on gender and age (±3 years).

None of the participants had a history of major head injury resulting in loss of consciousness, and MRI scans were without overt pathology as evaluated by a trained neuro-radiologist.

Clinical measures

All participants underwent comprehensive assessments at baseline including socio-demographics, psychopathology, level of functioning, and MRI.

The Structured Clinical Interview for DSM-IV Axis I Disorders (SCID-I) (First *et al.* 2001) and part of the Structured Clinical Interview for DSM-IV Axis II Disorders (SCID-II) (First *et al.* 1994) were used to diagnostically assess UHR individuals. All assessors (authors KK, DN, and LR) were certified SCID interviewers.

Positive symptoms were assessed with CAARMS (Yung *et al.* 2003, 2005), and all assessors had undergone formal CAARMS training. Negative symptoms were assessed with Scale for the Assessment of Negative Symptoms (SANS) (Andreasen, 1982). Level of functioning was assessed with the Social and Occupational Functioning Assessment Scale (SOFAS) (Goldman *et al.* 1992; Hilsenroth *et al.* 2000). Handedness was assessed using the Edinburgh Handedness Inventory (Oldfield, 1971).

Data on premorbid adjustment and systemic oxidative DNA and RNA damage in part of the UHR cohort has previously been published (Dannevang *et al.* 2016; Nordholm *et al.* 2016).

Image acquisition and processing

All MRIs were acquired in a 3 Tesla scanner (Philips Healthcare, Best, The Netherlands), using an 8-channel SENSE head coil (Invivo, Orlando, Florida, USA). Diffusion-weighted (DW) images were acquired using single shot spin-echo echoplanar imaging and a total of 31 different diffusion encodings: one diffusion un-weighted ($b = 0$ s/mm^2) and 30 diffusion weighted ($b = 1000$ s/mm^2) non-collinear directions. Acquired matrix size = 128 × 128 × 75; voxel dimensions = 1.88 × 1.88 × 2 mm^3 (slice gap = 0); TR = 7035 ms; TE = 68 ms; flip angle = 90°. Acquisition of each

https://doi.org/10.1017/S0033291717001210 Published online by Cambridge University Press

volume was repeated with opposite phase encoding direction enabling correction for susceptibility distortions (Andersson & Skare, 2002; Andersson *et al.* 2003). Foam-pads inside the head coil minimized head movement during scanning.

Tools from the FSL FMRIB software library v5.0.9 were used for image processing (Smith *et al.* 2004; Woolrich *et al.* 2009; Jenkinson *et al.* 2012). DW images were corrected for eddy current and head motion (Reese *et al.* 2003; Andersson & Sotiropoulos, 2015), and absolute and relative head motion measures were estimated. Next, a susceptibility artifact correction was performed (Andersson & Skare, 2002). Motion corrected data were interpolated to 1.33 × 1.33 × 2 voxel dimensions using sinc interpolation and non-brain tissue was removed with brain extraction tool (BET) (Smith, 2002). DTIFIT was used to calculate the diffusion parameter maps of FA, AD, RD, and MO and residual maps. The tract-based spatial statistics (TBSS) tool in FSL (Smith *et al.* 2004, 2006) was used to align FA data using the nonlinear image registration tool (FNIRT) (Andersson *et al.* 2007*a*, *b*). The resulting mean FA image (threshold of 0.2) was thinned to create a mean FA skeleton, which represented the centers of all tracts common to the group. Next, the nearest maximum FA values of each registered FA image were projected onto the mean FA skeleton. AD, RD, and MO were also skeletonized by projecting onto the FA skeleton. The skeletonized images were corrected for absolute and relative head motion (in scanner), age, gender, parental socioeconomic status, antipsychotic medication, tobacco smoking, alcohol- and drug use using fsl_glm, and the residuals were *z*-transformed by subtracting the voxelwise mean and dividing by the voxelwise standard deviation across UHR individuals and HCs (Geladi & Kowalski, 1986).

MRI quality metrics

Quality control was done by visually inspecting all DW images slice by slice before processing and all squared residual maps that were created after calculating the DTI derived parameters maps. Additionally, four quality metrics [mean voxel intensity outlier count (MEANVOX), maximum voxel intensity outlier count (MAXVOX), mean relative head motion, and temporal signal-to-noise ratio (TSNR)] were computed from each DW image using a quality assessment method (Roalf *et al.* 2016). Accordingly, these metrics were compared with standardized values in three different quality groups. In general, the quality metrics in the present study ranged between the 'good' and 'excellent' quality assessment group. For details see online Supplementary Table S1. Differences in absolute- and relative head motion (in scanner) summary measures between UHR individuals and HCs are provided in Table 1.

Statistical analysis on sociodemographic and clinical data

Statistical Package for the Social Sciences software (version 22.0, SPSS Inc., USA) was used to analyze demographic and clinical data. Distribution of continuous data was tested for normality with the Kolmogorov-Smirnov test. Since data on age, years of education, height, and weight were not normally distributed group comparisons were performed non-parametrically using the Mann–Whitney *U* test. Data on absolute- and relative head motion summary measures were normally distributed and analyzed with independent samples *t* test. Ordinal data such as tobacco smoking, alcohol and drug use were tested using the Mann–Whitney *U* test. Handedness was assessed using Pearson's χ^2 test. Gender differences and parental socioeconomic status were assessed using Fisher's exact test.

A positive symptom severity score was calculated as the summed scores of the product of global rating scale scores (0–6) and frequency (0–6) scores of the four subscales of CAARMS (Morrison *et al.* 2012). A negative symptom severity score was calculated by averaging the global scores on the first four items of the SANS leaving out the attention global score (Arndt *et al.* 1995).

Statistical analysis of MRI data using multivariate PLSC

Multivariate Partial Least Squares correlation analysis (PLSC) [graphical user interface, Rotman Research Institute, Baycrest Centre, University of Toronto; downloaded from http://www.rotman-baycrest.on.ca/pls/ running on MATLAB R2013b (MathWorks, Inc., Natick, Massachusetts, USA)] was used to explore group differences in DTI parameters (i.e. FA, AD, RD, and MO at each voxel) between UHR individuals and HCs and to analyze co-variations between DTI parameters and clinical measures (i.e. CAARMS, SANS, and SOFAS) within the UHR individuals.

In the group analyses 'mean-centered task PLSC' (Krishnan *et al.* 2011; Guitart-Masip *et al.* 2016) was employed. DTI parameters of both UHR individuals and HCs were stored in a matrix denoted X, with rows representing participants and DTI parameters and columns representing spatial locations (i.e. voxels) within a brain mask. Using task PLSC a matrix R was constructed, so that each row contained the average of one parameter within one group. In the present case, R therefore had eight rows (four DTI parameters × two groups). After singular value decomposition (SVD)

https://doi.org/10.1017/S0033291717001210 Published online by Cambridge University Press

Table 1. *Demographics and clinical characteristics of participants*

Variable	UHR individuals *N*/Mean %/S.D.		Healthy controls *N*/Mean %/S.D.		*p* value
Gender	(*N* = 45)		(*N* = 45)		1.00[a]
• Female	23	51.1	23	51.1	
• Male	22	49.9	22	49.9	
Age	(*N* = 45) 23.71	4.65	(*N* = 45) 23.80	5.15	0.913[b]
• Range	19–38		18–41		
Years of education	(*N* = 45) 12.97	2.91	(*N* = 45) 14.18	2.44	0.023[b]
• Range	3–21		10–21		
Parental socioeconomic status	(*N* = 45)		(*N* = 44)		0.001[a]
• 1 (high)	28	62.2	13	29.5	
• 2 (middle)	17	37.8	26	59.1	
• 3 (low)	0	0	5	11.4	
Height in cm	(*N* = 45) 174.61	9.98	(*N* = 27) 178.50	8.45	0.056[b]
• Range	160–195		164–192		
Weight in kg	(*N* = 45) 76.27	20.73	(*N* = 38) 69.23	14.67	0.113[b]
• Range	46–137		52–120		
Handedness	(*N* = 44)		(*N* = 44)		0.536[c]
• right	42	95.5	40	90.9	
• left	2	4.5	3	6.8	
• ambidextrous	0	0	1	2.3	
Alcohol consumption	(*N* = 45)		(*N* = 45)		0.169[b]
• never	2	4.4	2	4.4	
• few times	5	11.1	1	2.2	
• regular use	28	62.2	42	93.3	
• abuse	7	15.6	0	0	
• dependency	3	6.7	0	0	
Tobacco smoking	(*N* = 45)		(*N* = 44)		<0.001[b]
• never	7	15.6	12	27.3	
• few times	9	20	21	47.7	
• regular use	15	33.3	10	22.7	
• abuse	2	4.4	1	2.3	
• dependency	12	26.7	0	0	
Drug use	(*N* = 45)		(*N* = 45)		<0.001[b]
• never	8	17.8	18	40.0	
• few times	18	40.0	24	53.3	
• regular use	8	17.8	3	6.7	
• abuse	4	8.9	0	0	
• dependency	7	15.6	0	0	
Medication	(*N* = 45)				
• lifetime antipsychotic	9	20	–	–	–
• current antipsychotic	7	15.6	–	–	–
• current antidepressant	12	26.7	–	–	–
• current mood stabilizers	0	0	–	–	–
• current benzodiazepines	0	0	–	–	–
CAARMS subgroups	(*N* = 45)				
• APS	19	42.2	–	–	–

https://doi.org/10.1017/S0033291717001210 Published online by Cambridge University Press

Table 1 (*cont.*)

Variable	UHR individuals *N*/Mean %/S.D.		Healthy controls *N*/Mean %/S.D.		*p* value
• BLIPS	0	0	–	–	–
• TS	2	4.4	–	–	–
• APS + BLIPS	1	2.2	–	–	–
• APS + TS	21	46.7	–	–	–
• APS + BLIPS + TS	2	4.4	–	–	–
• TS + BLIPS	0	0	–	–	–
CAARMS	(*N* = 45) 47.67	14.88	–	–	–
SOFAS	(*N* = 45) 44.69	7.36	–	–	–
SANS	(*N* = 45) 1.82	0.65	–	–	–
MRI – absolute motion	(*N* = 45) 1.604	0.199	(*N* = 45) 1.462	0.302	0.010[d]
MRI – relative motion	(*N* = 45) 0.684	0.173	(*N* = 45) 0.627	0.148	0.100[d]

Table 1 shows demographics and clinical characteristics of participants

Drug use, Cannabis, opioids, hallucinogens, stimulants, other illicit drugs; Medication, UHR Individuals could be taking a combination of the listed compounds; APS, attenuated psychotic symptoms; BLIPS, brief limited intermittent psychotic symptoms; TS, trait and state; CAARMS, Comprehensive Assessment of At-Risk Mental States; SOFAS, Social and Occupational Functioning Assessment Scale; SANS, Scale for the Assessment of Negative Symptoms

[a] Fisher exact test

[b] Mann Whitney *U*

[c] Pearsons χ^2

[d] Independent samples *t* test.

latent variables (LVs) were calculated by projecting the left and right singular vectors onto the X and design matrices. This produced eight pairs of LVs with corresponding singular values [representing the proportion of the covariance accounted for by that given LV (the cross-block covariance)] and voxel saliences (indicating the degree to which each voxel was related to the effect characterized by that LV).

In the analysis exploring co-variations within UHR individuals the DTI parameters and clinical measures were considered two different data-blocks, each represented in matrix form. The DTI data block was represented by a matrix X, which was structured as the one used in the group analysis however only including the UHR individuals. The clinical measures were represented by a matrix Y, in which rows represented UHR individuals and columns represented clinical measures. The clinical measures were repeated to obtain the same no. of rows as in the DTI data block. Using 'behavior PLSC' a cross-correlation matrix (R) was computed by estimating the covariance between X and Y. SVD of R was then performed, and by projecting the resulting left and right singular vectors onto the X or Y matrices 12 pairs of LVs (four DTI parameters × three clinical measures) (McIntosh *et al.* 1996; Krishnan *et al.* 2011) with corresponding singular values and voxel saliences were computed.

Significance of the LVs was assessed using permutation tests. This involved a Monte-Carlo like procedure in which a new data set (permutation sample) was obtained by randomly reordering the rows of X but leaving Y/design matrix unchanged (McIntosh *et al.* 1996; McIntosh & Lobaugh, 2004). The permutation sample was then recomputed in the PLSC model thereby obtaining new singular values. This procedure was repeated 5000 times and the likelihood that the singular values obtained in the original analysis were due to random chance was determined (McIntosh *et al.* 1996; McIntosh & Lobaugh, 2004).

Stability and reliability of the voxel saliences was determined using bootstrap resampling (Krishnan *et al.* 2011). In this procedure a new data set (bootstrap

https://doi.org/10.1017/S0033291717001210 Published online by Cambridge University Press

sample) was obtained by resampling with replacement the rows of both X and Y/design matrix. The procedure was repeated 500 times, and the standard error of the saliences at each voxel was estimated. Bootstrap ratios were obtained by dividing each voxels salience by its standard error. Saliences with bootstrap ratios greater than ±1.96 were considered reliable since bootstrap ratios are roughly analogous to *Z* scores (a *Z* score of 1.96 has $p < 0.05$, two-tailed) (Grady *et al.* 2000; Ziegler *et al.* 2013; Cha *et al.* 2015). We reported reliable bootstrap clusters (cluster size $\geqslant 25$ voxels) (Ersche *et al.* 2013) with positive and negative correlations to the pattern seen in LV. Coordinates in all tables were extracted from JHU WM tractography atlas provided by FSL (Mori & van, 2007; Wakana *et al.* 2007; Hua *et al.* 2008) and reported in Montreal Neurological Institute (MNI) co-ordinates.

Statistical analysis of MRI data using univariate voxelwise analysis and ROI

In order to confirm the direction and localization of the PLSC findings we used univariate voxelwise analysis to compare DTI maps (FA, AD, MO, RD, and MD) between UHR individuals and HCs, and correlated the DTI maps to positive and negative symptoms (CAARMS and SANS) and level of functioning (SOFAS) within the UHR individuals. The univariate analysis were performed non-parametrically using the randomize function (5000 permutations) from the FSL FMRIB software library v5.0.9 (https://fsl.fmrib.ox.ac.uk/fsl/fslwiki) (Smith *et al.* 2004; Woolrich *et al.* 2009; Jenkinson *et al.* 2012). Family-wise error correction (Bullmore *et al.* 1999) with a threshold of $p < 0.05$ was used to correct for multiple comparisons and threshold-free cluster enhancement (Smith & Nichols, 2009) was applied to enhance cluster-like structures but keeping the images fundamentally voxelwise. The anatomical locations of significant regions were identified in MNI co-ordinates using the JHU WM tractography atlas (Mori & van, 2007; Wakana *et al.* 2007; Hua *et al.* 2008).

To quantify the results found in the PLSC analysis we used the three largest reliable spatial regions with positive correlations and the largest reliable spatial region with negative correlations to the pattern in LV1 as ROIs. Mean FA, AD, MO, and RD in these ROIs were compared between UHR individuals and HCs.

Results

Two of the 50 individuals included in the study were not MRI scanned due to dental braces, two did not undergo the DTI-sequences due to technical problems, and one had to be excluded from analyses due to poor MRI quality. Thus, 45 UHR individuals were included in the current analyses. Forty-five HCs were included; however, in one HC only one of the two DWI acquisitions could be used.

Sample characteristics

The UHR individuals and HCs did not differ significantly regarding handedness, height, weight, alcohol consumption, or use of benzodiazepines. The groups differed significantly in years of education, parental socioeconomic status, tobacco smoking, and drug abuse. Demographic and clinical data are presented in Table 1.

WM differences between UHR and HCs

Multivariate PLSC analysis of UHR individuals *v.* HCs identified one significant LV with $p < 0.001$ accounting for 52% of the cross-block covariance. This LV showed a pattern where the UHR individuals had lower FA, AD, and MO along with higher RD in widespread brain regions (displayed in red-yellow color in Fig. 1). One smaller region showed the inverse pattern with higher FA, AD, and MO along with lower RD (displayed in blue color in Fig. 1). Each DTI parameter contributed significantly to this pattern as demonstrated by the error-bars (based on bootstrapping); see Fig. 1 and Table 2.

Univariate voxelwise analyses of UHR individuals *v.* HCs found significantly lower FA in the UHR individuals in brain regions involving the superior longitudinal fasciculus, inferior fronto-occipital fasciculus, and anterior thalamic radiation. No significant voxelwise differences in AD, MO, and RD maps between UHR individuals and HCs were found. See online Supplementary Fig. S1.

When quantifying the PLSC results we compared mean FA, AD, MO, and RD in UHR individuals *v.* HCs in the three largest reliable clusters (used as ROIs) found by PLSC with positive correlations and the largest cluster with negative correlations (only one was identified) to the pattern in LV. This showed significantly different mean values for the majority of DTI parameters. See online Supplementary Table S2.

Associations between DTI parameters and clinical measures

Multivariate PLSC analysis correlating DTI parameters to clinical scores revealed five significant LVs (all permuted *p* values < 0.03). LV1–LV5 accounted for 31, 18, 15, 8, and 5% of the cross-block covariance, respectively. Since LV1 explained a considerably larger proportion of the cross-block covariance, only LV1 is

https://doi.org/10.1017/S0033291717001210 Published online by Cambridge University Press

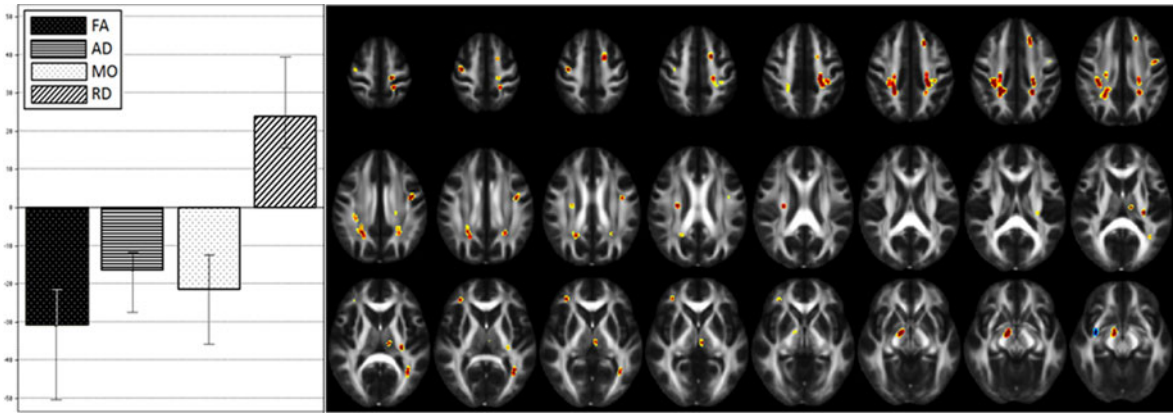

Fig. 1. Multivariate analysis of white matter differences between UHR and healthy controls. It shows white matter differences between UHR individuals and healthy controls. The panel to the left shows the pattern identified by LV1, in which UHR individuals have lower FA, AD, and MO concomitant with higher RD than healthy controls. In the panel to the right the most reliable spatial regions demonstrating this pattern (i.e. positive bootstrap-ratios) are highlighted in red-yellow color. Spatial regions demonstrating the inverse pattern (i.e. negative bootstrap ratios) are highlighted in blue color. Only clusters with bootstrap ratios greater than ±1.96 and cluster size ⩾25 voxels are shown. The brain is displayed according to radiological convention (participant's left is to the right) and in axial slices. Clusters are enhanced using tbss_fill (FSL version 5.09).

reported here. The pattern identified by LV1 showed that more positive and negative symptoms (i.e. high CAARMS and SANS scores) and low levels of functioning (i.e. low SOFAS scores) were correlated to lower FA, AD, MO, and higher RD (regions displayed in red-yellow color in Fig. 2). A few brain regions demonstrated the inverse correlations with more positive and negative symptoms (i.e. high CAARMS and SANS scores) combined with low levels of functioning (i.e. low SOFAS scores) being correlated to higher FA, AD, MO, and lower RD (regions displayed in blue color in Fig. 2). The error-bars (based on bootstrapping) in Fig. 2 show that each DTI parameter contributes significantly to the pattern in LV1. See Fig. 2 and Table 3.

Univariate voxelwise analysis correlating DTI maps to positive and negative symptoms (CAARMS and SANS) and level of functioning (SOFAS) showed that SOFAS was significantly positively correlated to FA in brain regions involving the left inferior longitudinal fasciculus, that SOFAS was positively correlated to AD in brain regions involving the left inferior fronto-occipital fasciculus and the right superior longitudinal fasciculus, and that SOFAS was positively correlated to MO in brain regions involving the right inferior fronto-occipital fasciculus, the left superior longitudinal fasciculus, and the right anterior thalamic radiation. No significant correlations between SOFAS and RD, and MD were found, and SOFAS was not significantly negatively correlated to any of the DTI parameters. Neither SANS nor CAARMS was significantly correlated (positively or negatively) to any of the DTI parameters. See online Supplementary Fig. S2.

Discussion

The present study is the first to use PLSC to explore WM microstructure in UHR individuals. In the PLSC group analysis one pattern of DTI parameters could significantly differentiate UHR individuals from matched HCs. This pattern indicated that UHR individuals had lower FA, AD, MO, and higher RD in widespread brain regions compared with HCs. Similar findings of low FA concomitant with high RD have been reported in several studies in UHR, in studies of first-episode of psychosis, and in studies of chronic schizophrenia (von Hohenberg *et al.* 2014; Spalletta *et al.* 2015; Zhu *et al.* 2015; Li *et al.* 2016; van Dellen *et al.* 2016; Zeng *et al.* 2016). Findings of low AD are more scarce, and have been reported in genetic- and clinical high-risk cohorts (Kikinis *et al.* 2013; Rigucci *et al.* 2016) and in early psychosis (Hatton *et al.* 2014).

In DTI, the most frequently used summary measure is FA. However, other DTI parameters such as AD, RD, and MO may reflect more distinct aspects of WM microstructure (Aung *et al.* 2013). Axonal damage such as axonal swelling (Song *et al.* 2005; Kim *et al.* 2010) or diffuse axonal injury (Arfanakis *et al.* 2002; Li *et al.* 2011; Bennett *et al.* 2012) has been shown to be reflected by a decrease in AD. Demyelination has been associated with an increase in RD (Song *et al.* 2002, 2005; Harsan *et al.* 2006; Sun *et al.* 2006*a*, *b*; Xie *et al.* 2010) sometimes preceded or accompanied by a decrease in AD probably due to minor axonal damage early in the demyelination process (Harsan *et al.* 2006; Sun *et al.* 2006*b*; Tyszka *et al.* 2006). We speculate that our findings of high RD accompanied by low AD could reflect abnormalities in the myelination process,

https://doi.org/10.1017/S0033291717001210 Published online by Cambridge University Press

Table 2. *Multivariate analysis of white matter differences between UHR and healthy controls*

Brain regions with positive correlations to LV1 (↓FA, ↓AD, ↓MO, ↑RD in UHR)	Hemisphere left/right	Number of voxels	X^a	Y^a	Z^a	Boots-trap ratio
Cingulum (cingulate gyrus)	R	304	17	−42	41	3.17
Corticospinal tract	L	203	−21	−28	40	3.11
Superior longitudinal fasciculus	R	134	31	−32	40	3.38
Anterior thalamic radiation	R	108	10	−4	−7	3.15
Inferior fronto-occipital fasciculus	L	86	−22	−44	39	3.18
Superior longitudinal fasciculus	L	67	−40	−5	36	2.83
Inferior fronto-occipital fasciculus	L	62	−35	−57	7	3.06
Corticospinal tract	L	57	−12	−26	65	3.66
Superior longitudinal fasciculus	R	51	33	−15	57	3.85
Cingulum	L	48	−16	21	42	2.72
Unknown	NA	44	−15	2	52	2.70
Anterior thalamic radiation	R	41	34	38	5	3.43
Corticospinal tract	L	34	−17	−37	59	2.59
Superior longitudinal fasciculus	L	34	−28	−28	47	2.59
Corticospinal tract	L	34	−27	−23	11	2.95
Anterior thalamic radiation	L	34	−3	−19	1	3.36
Corticospinal tract	R	33	21	−25	42	2.76
Anterior thalamic radiation	L	28	−11	−19	13	3.13
Inferior longitudinal fasciculus	L	27	−34	−43	−16	2.69
Corticospinal tract L	R	27	28	−17	26	3.15
Inferior fronto-occipital fasciculus L	R	25	27	−77	4	3.33
Brain regions with negative correlations to LV1 (↑FA, ↑AD, ↑MO, ↓RD in UHR)	**Hemisphere left/right**	**Number of voxels**	X^a	Y^a	Z^a	**Boots-trap ratio**
Uncinate fasciculus	R	56	37	−6	−14	−3.54

NA, not applicable

Table 2 shows the most reliable spatial brain regions with white matter differences between UHR individuals and healthy controls. In regions with positive correlations to the pattern in LV1 (i.e. positive bootstrap-ratios) the UHR individuals have: ↓FA, ↓AD, ↓MO, ↑RD compared with healthy controls, and in regions with negative correlations (i.e. negative bootstrap-ratios) to the pattern in LV1 the UHR individuals have: ↑FA, ↑AD, ↑MO, ↓RD compared with healthy controls. Only regions with bootstrap ratios greater than ±1.96 and cluster size ⩾25 voxels are displayed

Localization is performed using FSL

[a] Local maxima in MNI coordinates (mm) are extracted from JHU WM tractography atlas

which could in turn sub-serve the observed symptomatology. In our study, the abnormalities in FA, AD, and RD were accompanied by abnormalities in MO. This is in agreement with previous studies finding an association between low FA, high RD, and low MO in patients with schizophrenia (Kumar *et al.* 2015; Wigand *et al.* 2015). Since MO has been found to be low in regions of crossing fibers from two fiber populations and high in regions where only one fiber orientation predominates (Ennis & Kindlmann, 2006; Kindlmann *et al.* 2007; Wigand *et al.* 2015) our findings could be indicative of aberrations in the underlying fiber structure in UHR individuals.

In the PLSC analysis associating DTI parameters to symptoms within the UHR individuals, the pattern explaining the largest proportion of the cross-block covariance (LV1) indicated that severity of symptoms was negatively correlated to FA, AD, MO, and positively to RD in the majority of identified brain regions. The negative correlation between positive symptoms and FA is in accordance with findings in other studies of UHR individuals (Bloemen *et al.* 2010), individuals experiencing sub-threshold psychotic symptoms (Cooper *et al.* 2016), and patients with first-episode psychosis and chronic schizophrenia (Skelly *et al.* 2008; Catani *et al.* 2011; Cui *et al.* 2011; Boos *et al.* 2013; Hatton *et al.* 2014; Ohtani *et al.* 2015; Ebdrup *et al.* 2016; Seitz *et al.* 2016; Zhang *et al.* 2016). Of note, these studies find a negative correlation between positive symptoms and FA in some of the same areas where we also find a negative correlation namely the left and right superior longitudinal fasciculus (Skelly *et al.* 2008; Ebdrup *et al.* 2016) and the right inferior longitudinal fasciculus (Seitz *et al.* 2016). Most of the

https://doi.org/10.1017/S0033291717001210 Published online by Cambridge University Press

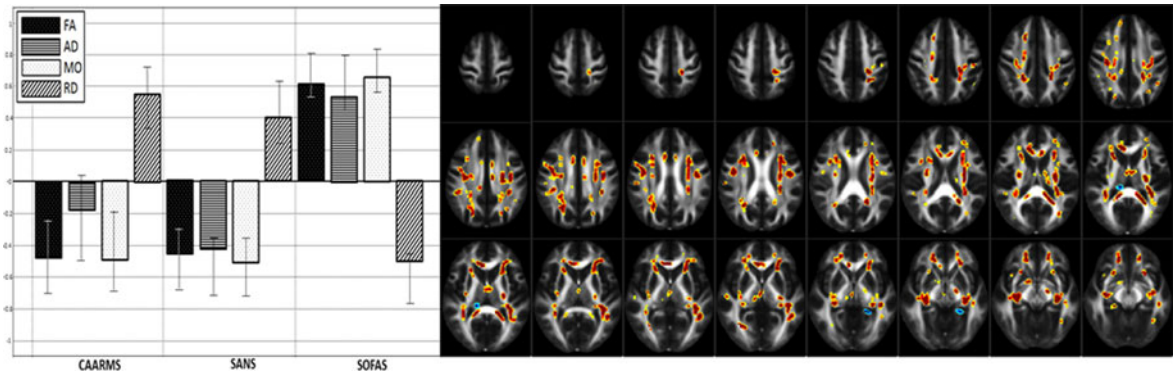

Fig. 2. Multivariate analysis associating white matter to symptoms and level of functioning within UHR individuals. It shows the associations found by LV1 between DTI parameters, symptoms (CAARMS and SANS), and level of functioning (SOFAS) within the UHR individuals. The panel to the left shows the pattern identified by LV1 in which more positive and negative symptoms (high CAARMS and SANS scores) and low levels of functioning (low SOFAS scores) are correlated to ↓FA, ↓AD, ↓ MO and ↑ RD. In the panel to the right the most reliable spatial regions demonstrating this pattern (i.e. positive bootstrap-ratios) are highlighted in red-yellow color. Spatial regions demonstrating the inverse pattern (i.e. negative bootstrap ratios) are highlighted in blue color. Only clusters with bootstrap ratios greater than ±1.96 and cluster size ⩾25 voxels are shown. The brain is displayed according to radiological convention (participant's left is to the right) and in axial slices. Clusters are enhanced using tbss_fill (FSL version 5.09).

studies only report on FA, but a few studies also report a positive correlation between positive symptoms and RD and a negative correlation between positive symptoms and MO (Wigand *et al.* 2015; Seitz *et al.* 2016).

Our findings of a negative correlation between severity of negative symptoms and FA are consistent with many studies in first-episode of psychosis and schizophrenia (Wolkin *et al.* 2003; Szeszko *et al.* 2008; Asami *et al.* 2014; Ohtani *et al.* 2015; Sun *et al.* 2015; Zeng *et al.* 2016). Collectively, our data add to the notion that in UHR individuals, abnormal WM microstructure in widespread brain regions may underlie both positive and negative symptoms and low levels of functioning.

Study limitations

Although our sample is larger than those in most previous DTI studies in UHR individuals, statistical power may still be limited. We addressed this by using PLSC, which limits the need for correction for multiple comparisons (McLelland *et al.* 2014; Protzner *et al.* 2016). By means of this non-biased approach, we identified clinical meaningful significant group differences as well as with-in group associations. The identified regional overlaps with previous studies of patients with schizophrenia at different stages of illness, add to the external validity of our data-driven, whole brain findings. The UHR individuals and HCs were matched on gender and age (±3 years), however, as could be expected the groups differed in terms of years of education, parental socioeconomic status, tobacco smoking, and drug use. Of these, especially tobacco smoking and drug use could represent potential confounding factors. Effects of tobacco smoking on WM have shown equivocal results. Some studies have reported high FA (Jacobsen *et al.* 2007; Paul *et al.* 2008; Liao *et al.* 2011; Hudkins *et al.* 2012; Huang *et al.* 2013; van Ewijk *et al.* 2015; Viswanath *et al.* 2015; Yu *et al.* 2016), but tobacco use has been associated with low FA in other studies (Lin *et al.* 2013; Savjani *et al.* 2014; Umene-Nakano *et al.* 2014; Baeza-Loya *et al.* 2016). Moreover, it has been suggested that the effect of nicotine may differ across the lifespan with FA increase in young (age < 30 years) and FA decrease in older smokers (Gogliettino *et al.* 2016). Long-term use of drugs such as cannabis (Ashtari *et al.* 2009; Bava *et al.* 2009; Yucel *et al.* 2010; James *et al.* 2011; Zalesky *et al.* 2012), inhalants (Yucel *et al.* 2010), and cocaine (Lim *et al.* 2002; Moeller *et al.* 2005; Ma *et al.* 2009; Lane *et al.* 2010; Narayana *et al.* 2014) has primarily been associated to low FA and high RD. *Post hoc* analyses comparing the subgroup of 26 UHR individuals, who never had an abuse or dependency of alcohol, drugs, or tobacco to the HCs revealed a significant ($p < 0.001$) pattern similar to the one seen in the analysis including all 45 UHR individuals, suggesting that these confounders have not substantially influenced the present results. See online Supplementary Fig. S3.

Some of the UHR individuals had received antipsychotic medication, although in very modest cumulative lifetime doses (not exceeding 50 mg haloperidol or equivalent other antipsychotic medication). *Post hoc* analyses comparing the subgroup of 36 UHR individuals, who had never taken antipsychotic medication to the HCs revealed a significant ($p < 0.001$)

https://doi.org/10.1017/S0033291717001210 Published online by Cambridge University Press

Table 3. *Multivariate analysis associating white matter to symptoms and level of functioning within UHR individuals*

Brain regions with positive correlations to LV1	Hemisphere left/right	Number of voxels	X^a	Y^a	Z^a	Boots-trap ratio
Superior longitudinal fasciculus	L	1759	−40	−13	27	5.88
Inferior fronto-occipital fasciculus	L	696	−33	−36	9	5.54
Superior longitudinal fasciculus	R	542	25	−61	32	4.88
Superior longitudinal fasciculus	R	529	43	−11	27	4.49
Inferior fronto-occipital fasciculus	R	428	33	−18	−9	5.15
Superior longitudinal fasciculus	L	365	−22	−40	42	4.62
Forceps minor		353	11	30	12	5.58
Forceps major		314	−21	−50	14	6.58
Inferior fronto-occipital fasciculus	R	245	22	22	4	4.47
Anterior thalamic radiation	L	229	−17	−22	19	4.96
Forceps minor		205	16	36	−13	4.78
Inferior fronto-occipital fasciculus	L	198	−29	−24	−8	4.26
Superior longitudinal fasciculus	R	192	30	12	35	4.12
Inferior fronto-occipital fasciculus	R	190	36	−42	6	4.93
Inferior longitudinal fasciculus	L	136	−40	−53	2	6.09
Unknown		119	25	−34	−28	3.63
Uncinate fasciculus	L	108	−16	39	−9	5.16
Forceps major		89	16	−42	12	5.44
Superior longitudinal fasciculus	R	87	50	−40	32	4.17
Superior longitudinal fasciculus	R	86	28	−11	22	3.23
Inferior longitudinal fasciculus	L	80	−46	−27	−15	4.32
Corticospinal tract	L	78	−11	−67	−27	3.79
Cingulum (cingulate gyrus)	R	78	9	14	30	6
Superior longitudinal fasciculus	R	77	32	8	26	4.48
Inferior fronto-occipital fasciculus	L	75	−36	−13	−10	3.94
Cingulum (cingulate gyrus)	L	73	−7	5	33	4.24
Uncinate fasciculus	R	70	23	15	−12	4.12
Superior longitudinal fasciculus	L	69	−32	−37	35	3.81
Forceps minor		68	−27	41	14	3.81
Anterior thalamic radiation	L	66	−25	−33	8	3.42
Corticospinal tract	R	58	20	−12	41	3.34
Superior longitudinal fasciculus	R	58	19	21	39	2.69
Inferior fronto-occipital fasciculus	R	57	27	33	0	3.96
Inferior longitudinal fasciculus	R	55	34	−62	2	3.37
Superior longitudinal fasciculus	R	48	50	3	31	3.54
Corticospinal tract	L	47	−10	−28	−21	3.98
Forceps minor		46	−10	23	19	3.38
Cingulum (cingulate gyrus)	L	44	−7	−15	35	4.07
Cingulum (hippocampus)	R	44	26	−32	−13	3.72
Anterior thalamic radiation	R	43	15	5	−7	3.39
Anterior thalamic radiation	R	43	3	−17	2	4.23
Uncinate fasciculus	L	40	−22	17	−10	5.05
Unknown		39	36	−71	−32	3.22
Cingulum (cingulate gyrus)	L	39	−17	−43	33	4.14
Corticospinal tract	L	37	−16	−12	−6	3.09
Superior longitudinal fasciculus	R	36	55	−24	27	5.02
Inferior longitudinal fasciculus	L	35	−34	5	−32	3.36
Inferior longitudinal fasciculus	L	34	−44	1	−22	4.75
Corticospinal tract	L	34	−12	−53	−26	4.12
Inferior fronto-occipital fasciculus	R	33	34	−79	14	4.24
Superior longitudinal fasciculus	R	32	38	14	−10	5.49
Superior longitudinal fasciculus	L	32	−32	4	18	3.46
Inferior longitudinal fasciculus	L	32	−21	−68	33	5.76
Superior longitudinal fasciculus	L	31	−29	−61	38	3.84

https://doi.org/10.1017/S0033291717001210 Published online by Cambridge University Press

Table 3 (*cont.*)

Brain regions with positive correlations to LV1	Hemisphere left/right	Number of voxels	X^a	Y^a	Z^a	Boots-trap ratio
Anterior thalamic radiation	R	31	11	−23	1	4.27
Inferior longitudinal fasciculus	L	30	−33	−71	17	3.2
Inferior longitudinal fasciculus	R	29	54	−18	2	4.42
Anterior thalamic radiation	R	29	27	28	16	3.3
Inferior fronto-occipital fasciculus	L	29	−34	36	7	3.67
Inferior fronto-occipital fasciculus	L	28	−29	−21	2	3.41
Superior longitudinal fasciculus	L	28	−43	−49	39	3.41
Corticospinal tract	L	27	−14	−61	−28	3.42
Superior longitudinal fasciculus	R	27	28	−38	39	3.34
Inferior longitudinal fasciculus	L	27	−37	−55	−11	3.86
Cingulum (cingulate gyrus)	R	27	10	36	14	4.22
Cingulum (cingulate gyrus)	R	26	11	−33	36	3.69
Forceps minor		26	13	41	36	3.26
Inferior fronto-occipital fasciculus	R	26	40	−22	−6	3.31
Forceps minor		26	−16	35	26	3.52
Uncinate fasciculus	L	25	−41	10	−26	3.48
Superior longitudinal fasciculus	R	25	46	−38	19	4.11
Inferior fronto-occipital fasciculus	R	25	25	−67	2	3.28
Anterior thalamic radiation	R	25	22	36	9	2.85
Superior longitudinal fasciculus	L	25	−45	−22	45	3.38
Brain regions with negative correlations to LV1	**Hemisphere left/right**	**Number of voxels**	X^a	Y^a	Z^a	**Boots-trap ratio**
Corticospinal tract	L	166	−8	−27	−33	−4.49
Anterior thalamic radiation	R	51	7	−40	−25	−3.65
Cingulum (hippocampus)	L	48	−22	−42	−4	−3.88
Anterior thalamic radiation	R	39	15	−31	12	−2.92
Corticospinal tract	L	32	−13	−19	−15	−3.72

NA, not applicable

Table 3 shows the most reliable spatial brain regions in which DTI parameters are correlated to symptoms (CAARMS and SANS), and level of functioning (SOFAS) within the UHR individuals. In regions with positive correlations (i.e. positive bootstrap-ratios) to the pattern in LV1, more positive and negative symptoms (i.e. high CAARMS and SANS scores) and low levels of functioning (i.e. low SOFAS scores) are correlated to ↓FA, ↓AD, ↓MO, and ↑RD, while regions with negative correlations (i.e. negative bootstrap-ratios) to LV1 show the inverse pattern. Only brain areas with bootstrap ratios greater than ±1.96 and cluster size ⩾ 25 voxels are displayed

Localization is performed using FSL

[a] Local maxima in MNI coordinates (mm) are extracted from JHU WM tractography atlas

pattern similar to the one found in the analysis, including all 45 UHR individuals. See online Supplementary Fig. S4. *Post hoc* analyses comparing the subgroup of 33 UHR individuals who did not take antidepressant medication to the HCs showed a significant pattern ($p < 0.001$) similar to the one including all 45 UHR individuals. See online Supplementary Fig. S5. These findings suggest that exposure to neither antipsychotic nor antidepressant medication substantially influenced the present results.

Interpretation of DTI findings can be challenging. The measured diffusion effects are averaged over a voxel with much larger dimensions (measured in mm) than individual axons (measured in μm). Therefore, it can be difficult to disentangle signals reflecting aberrations in myelination from signals reflecting aberrations in fiber architecture, since both will influence RD and MO. Future MRI studies in UHR may benefit from combining DTI with other imaging contrasts, such as magnetization transfer ratio or myelin water fraction, which are putative measures of WM myelination (Mandl *et al.* 2015).

When visualizing the most reliable spatial regions showing the identified WM patterns we designated a bootstrap ratio threshold of ±1.96 (corresponding to approximately $p < 0.05$). However, since the PLSC

https://doi.org/10.1017/S0033291717001210 Published online by Cambridge University Press

uses the entire set of voxels as a single multivariate representation the exact extent and localization of the identified WM patterns are difficult to ascertain. We addressed this by doing additional univariate voxel-wise analysis and by quantifying the mean values of the DTI parameters in the largest spatial regions found by the PLSC (used as ROIs).

Since the contrast in DTI is generated by measuring the microscopic diffusion of water molecules in brain tissue it is sensitive to macroscopic head motion (Ling *et al.* 2012; Yendiki *et al.* 2014). It seems that more head motion is associated to an overestimation of RD and underestimation of AD and FA (Yendiki *et al.* 2014). In the present study foam-pads inside the scanner were used to minimize head motion, nevertheless more absolute but not relative head motion was observed in the UHR individuals compared with the HCs. No linear correlation was observed between relative head motion and CAARMS, SANS, or SOFAS [Pearson correlation = 0.006/0.049/−0.234 and p = 0.968/0.749/0.122 (2-sided)] or between absolute head motion and CAARMS or SANS [Pearson correlation = 0.167/0.110 and p = 0.272/0.941 (2-sided)]. However there was a significant correlation between absolute head motion and SOFAS [Pearson correlation = −0.298 and p = 0.047 (2-sided)]. We addressed this by visually inspecting all DW images before processing and discharging those where head motion led to visibly poor quality. Additionally DW images were corrected for eddy current and head-motion as part of the FSL processing pipeline, and furthermore we corrected for head motion parameters (absolute and relative) in both the univariate and the multivariate analysis.

Conclusion

In conclusion, we confirm the presence of subtle abnormalities in WM microstructure in UHR individuals with minimal antipsychotic exposure. The UHR individuals displayed a pattern of low FA, AD, and MO, concomitant with high RD compared with HCs. Within UHR individuals, the same pattern was associated to both positive and negative symptoms as well as level of functioning. Cerebral dysmyelination or aberrations in WM fiber architecture may play an important role in the emerging symptoms constituting a vulnerability for developing a psychotic disorder.

Supplementary material

The supplementary material for this article can be found at https://doi.org/10.1017/S0033291717001210.

Acknowledgements

Dr Ebdrup has received lecture fees and/or is part of Advisory Boards of Bristol-Myers Squibb, Eli Lilly and Company, Janssen-Cilag, Otsuka Pharma Scandinavia and Takeda Pharmaceutical Company. Dr Glenthøj is the leader of a Lundbeck Foundation Center of Excellence for Clinical Intervention and Neuropsychiatric Schizophrenia Research (CINS), which is partially financed by an independent grant from the Lundbeck Foundation based on international review and partially financed by the Mental Health Services in the Capital Region of Denmark, the University of Copenhagen, and other foundations. All grants are the property of the Mental Health Services in the Capital Region of Denmark and administrated by them. This work was supported by the Danish Council for Independent Research, Medical Sciences (DFF-4004-00314), the Lundbeck Foundation (R25-A2701 and R155-2013-16337), the University of Copenhagen (BHE, no grant number), and Mental Health Center Copenhagen (KK, no grant number).

Declaration of Interest

None.

Ethical Standard

The authors assert that all procedures contributing to this work comply with the ethical standards of the relevant national and institutional committees on human experimentation and with the Helsinki Declaration of 1975, as revised in 2008. The authors assert that all procedures contributing to this work comply with the ethical standards of the relevant national and institutional guides on the care and use of laboratory animals.

References

Andersson JL, Jenkinson M, Smith S (2007*a*). Non-linear optimisation. FMRIB technical report TR07JA1 from (http://www.fmrib.ox.ac.uk/analysis/techrep). In (Anonymous).

Andersson JL, Jenkinson M, Smith S (2007*b*). Non-linear registration, aka Spatial normalisation FMRIB technical report TR07JA2 from (http://www.fmrib.ox.ac.uk/analysis/techrep). In (Anonymous).

Andersson JL, Skare S (2002). A model-based method for retrospective correction of geometric distortions in diffusion-weighted EPI. *Neuroimage* **16**, 177–199.

Andersson JL, Skare S, Ashburner J (2003). How to correct susceptibility distortions in spin-echo echo-planar images: application to diffusion tensor imaging. *Neuroimage* **20**, 870–888.

Andersson JL, Sotiropoulos SN (2015). Non-parametric representation and prediction of single- and multi-shell

diffusion-weighted MRI data using Gaussian processes. *Neuroimage* **122**, 166–176.

Andreasen NC (1982). Negative symptoms in schizophrenia. Definition and reliability. *Archives of General Psychiatry* **39**, 784–788.

Andreasen NC, Pressler M, Nopoulos P, Miller D, Ho BC (2010). Antipsychotic dose equivalents and dose-years: a standardized method for comparing exposure to different drugs. *Biological Psychiatry* **67**, 255–262.

Arfanakis K, Haughton VM, Carew JD, Rogers BP, Dempsey RJ, Meyerand ME (2002). Diffusion tensor MR imaging in diffuse axonal injury. *AJNR American Journal of Neuroradiology* **23**, 794–802.

Arndt S, Andreasen NC, Flaum M, Miller D, Nopoulos P (1995). A longitudinal study of symptom dimensions in schizophrenia. Prediction and patterns of change. *Archives of General Psychiatry* **52**, 352–360.

Asami T, Hyuk LS, Bouix S, Rathi Y, Whitford TJ, Niznikiewicz M, Nestor P, McCarley RW, Shenton ME, Kubicki M (2014). Cerebral white matter abnormalities and their associations with negative but not positive symptoms of schizophrenia. *Psychiatry Research* **222**, 52–59.

Ashtari M, Cervellione K, Cottone J, Ardekani BA, Sevy S, Kumra S (2009). Diffusion abnormalities in adolescents and young adults with a history of heavy cannabis use. *Journal of Psychiatric Research* **43**, 189–204.

Aung WY, Mar S, Benzinger TL (2013). Diffusion tensor MRI as a biomarker in axonal and myelin damage. *Imaging in Medicine* **5**, 427–440.

Baeza-Loya S, Velasquez KM, Molfese DL, Viswanath H, Curtis KN, Thompson-Lake DG, Baldwin PR, Ellmore TM, De La Garza R, Salas R (2016). Anterior cingulum white matter is altered in tobacco smokers. *The American Journal on Addictions* **25**, 210–214.

Basser PJ, Pierpaoli C (2011). Microstructural and physiological features of tissues elucidated by quantitative-diffusion-tensor MRI. 1996. *Journal of Magnetic Resonance* **213**, 560–570.

Bava S, Frank LR, McQueeny T, Schweinsburg BC, Schweinsburg AD, Tapert SF (2009). Altered white matter microstructure in adolescent substance users. *Psychiatry Research* **173**, 228–237.

Bennett RE, Mac Donald CL, Brody DL (2012). Diffusion tensor imaging detects axonal injury in a mouse model of repetitive closed-skull traumatic brain injury. *Neuroscience Letters* **513**, 160–165.

Bernard JA, Orr JM, Mittal VA (2015). Abnormal hippocampal-thalamic white matter tract development and positive symptom course in individuals at ultra-high risk for psychosis. *NPJ. Schizophrenia* **1**, 15009.

Bloemen OJ, de Koning MB, Schmitz N, Nieman DH, Becker HE, de Haan L, Dingemans P, Linszen DH, van Amelsvoort TA (2010). White-matter markers for psychosis in a prospective ultra-high-risk cohort. *Psychological Medicine* **40**, 1297–1304.

Boos HB, Mandl RC, van Haren NE, Cahn W, van Baal GC, Kahn RS, Hulshoff Pol HE (2013). Tract-based diffusion tensor imaging in patients with schizophrenia and their non-psychotic siblings. *European Neuropsychopharmacology* **23**, 295–304.

Bullmore ET, Suckling J, Overmeyer S, Rabe-Hesketh S, Taylor E, Brammer MJ (1999). Global, voxel, and cluster tests, by theory and permutation, for a difference between two groups of structural MR images of the brain. *IEE Transactions on Medical Imaging* **18**, 32–42.

Caprihan A, Jones T, Chen H, Lemke N, Abbott C, Qualls C, Canive J, Gasparovic C, Bustillo JR (2015). The paradoxical relationship between white matter, psychopathology and cognition in schizophrenia: a diffusion tensor and proton spectroscopic imaging study. *Neuropsychopharmacology* **40**, 2248–2257.

Carletti F, Woolley JB, Bhattacharyya S, Perez-Iglesias R, Fusar PP, Valmaggia L, Broome MR, Bramon E, Johns L, Giampietro V, Williams SC, Barker GJ, McGuire PK (2012). Alterations in white matter evident before the onset of psychosis. *Schizophrenia Bulletin* **38**, 1170–1179.

Catani M, Craig MC, Forkel SJ, Kanaan R, Picchioni M, Toulopoulou T, Shergill S, Williams S, Murphy DG, McGuire P (2011). Altered integrity of perisylvian language pathways in schizophrenia: relationship to auditory hallucinations. *Biological Psychiatry* **70**, 1143–1150.

Cha J, Fekete T, Siciliano F, Biezonski D, Greenhill L, Pliszka SR, Blader JC, Roy AK, Leibenluft E, Posner J (2015). Neural correlates of aggression in medication-naive children with ADHD: multivariate analysis of morphometry and tractography. *Neuropsychopharmacology* **40**, 1717–1725.

Cheung V, Cheung C, McAlonan GM, Deng Y, Wong JG, Yip L, Tai KS, Khong PL, Sham P, Chua SE (2008). A diffusion tensor imaging study of structural dysconnectivity in never-medicated, first-episode schizophrenia. *Psychological Medicine* **38**, 877–885.

Cheung V, Chiu CP, Law CW, Cheung C, Hui CL, Chan KK, Sham PC, Deng MY, Tai KS, Khong PL, McAlonan GM, Chua SE, Chen E (2011). Positive symptoms and white matter microstructure in never-medicated first episode schizophrenia. *Psychological Medicine* **41**, 1709–1719.

Choi H, Kubicki M, Whitford TJ, Alvarado JL, Terry DP, Niznikiewicz M, McCarley RW, Kwon JS, Shenton ME (2011). Diffusion tensor imaging of anterior commissural fibers in patients with schizophrenia. *Schizophrenia Research* **130**, 78–85.

Cooper S, Alm KH, Olson IR, Ellman LM (2016). White matter alterations in individuals experiencing attenuated positive psychotic symptoms. *Early Intervention in Psychiatry*. Epub: doi:10.1111/eip.12306.

Cui L, Chen Z, Deng W, Huang X, Li M, Ma X, Huang C, Jiang L, Wang Y, Wang Q, Collier DA, Gong Q, Li T (2011). Assessment of white matter abnormalities in paranoid schizophrenia and bipolar mania patients. *Psychiatry Research* **194**, 347–353.

Dannevang AL, Randers L, Gondan M, Krakauer K, Nordholm D, Nordentoft M (2016). Premorbid adjustment in individuals at ultra-high risk for developing psychosis: a case-control study. *Early Intervention in Psychiatry*. Epub: doi: 10.1111/eip.12375.

DeRosse P, Ikuta T, Karlsgodt KH, Peters BD, Gopin CB, Szeszko PR, Malhotra AK (2016). White matter abnormalities associated with subsyndromal psychotic-like symptoms predict later social competence in children and adolescents. *Schizophrenia Bulletin* **43**, 152–159.

Ebdrup BH, Raghava JM, Nielsen MO, Rostrup E, Glenthoj B (2016). Frontal fasciculi and psychotic symptoms in antipsychotic-naive patients with schizophrenia before and after 6 weeks of selective dopamine D2/3 receptor blockade. *Journal of Psychiatry & Neuroscience* **41**, 133–141.

Ennis DB, Kindlmann G (2006). Orthogonal tensor invariants and the analysis of diffusion tensor magnetic resonance images. *Magnetic Resonance in Medicine* **55**, 136–146.

Epstein KA, Cullen KR, Mueller BA, Robinson P, Lee S, Kumra S (2014). White matter abnormalities and cognitive impairment in early-onset schizophrenia-spectrum disorders. *Journal of the American Academy of Child and Adolescent Psychiatry* **53**, 362–372.

Ersche KD, Williams GB, Robbins TW, Bullmore ET (2013). Meta-analysis of structural brain abnormalities associated with stimulant drug dependence and neuroimaging of addiction vulnerability and resilience. *Current Opinion in Neurobiology* **23**, 615–624.

Filippi M, Canu E, Gasparotti R, Agosta F, Valsecchi P, Lodoli G, Galluzzo A, Comi G, Sacchetti E (2014). Patterns of brain structural changes in first-contact, antipsychotic drug-naive patients with schizophrenia. *AJNR American Journal of Neuroradiology* **35**, 30–37.

First MB, Spitzer RL, Gibbon M, Williams J (2001). *Structured Clinical Interview for DSM-IV-TR Axis I Disorders (SCID I)*. Psychiatric Institute, Biometrics Research Department: New York State.

First MB, Spitzer RL, Gibbon M, Williams J, Benjamin L (1994). *Structured Clinical Interview for DSM-IV Axis II Personality Disorders (SCID II)*. Biometric Research Department: New York.

Gasparotti R, Valsecchi P, Carletti F, Galluzzo A, Liserre R, Cesana B, Sacchetti E (2009). Reduced fractional anisotropy of corpus callosum in first-contact, antipsychotic drug-naive patients with schizophrenia. *Schizophrenia Research* **108**, 41–48.

Geladi P, Kowalski BR (1986). Partial least-squares regression: a tutorial. *Analytica Chimica Acta* **185**, 1–17.

Gogliettino AR, Potenza MN, Yip SW (2016). White matter development and tobacco smoking in young adults: a systematic review with recommendations for future research. *Drug and Alcohol Dependence* **162**, 26–33.

Goldman HH, Skodol AE, Lave TR (1992). Revising axis V for DSM-IV: a review of measures of social functioning. *The American Journal of Psychiatry* **149**, 1148–1156.

Grady CL, McIntosh AR, Horwitz B, Rapoport SI (2000). Age-related changes in the neural correlates of degraded and nondegraded face processing. *Cognitive Neuropsychology* **17**, 165–186.

Guitart-Masip M, Salami A, Garrett D, Rieckmann A, Lindenberger U, Backman L (2016). BOLD variability is related to dopaminergic neurotransmission and cognitive aging. *Cerebral Cortex* **26**, 2074–2083.

Guo W, Liu F, Liu Z, Gao K, Xiao C, Chen H, Zhao J (2012). Right lateralized white matter abnormalities in first-episode, drug-naive paranoid schizophrenia. *Neuroscience Letters* **531**, 5–9.

Harsan LA, Poulet P, Guignard B, Steibel J, Parizel N, de Sousa PL, Boehm N, Grucker D, Ghandour MS (2006). Brain dysmyelination and recovery assessment by noninvasive *in vivo* diffusion tensor magnetic resonance imaging. *Journal of Neuroscience Research* **83**, 392–402.

Hatton SN, Lagopoulos J, Hermens DF, Hickie IB, Scott E, Bennett MR (2014). White matter tractography in early psychosis: clinical and neurocognitive associations. *Journal of Psychiatry & Neuroscience* **39**, 417–427.

Hilsenroth MJ, Ackerman SJ, Blagys MD, Baumann BD, Baity MR, Smith SR, Price JL, Smith CL, Heindselman TL, Mount MK, Holdwick Jr. DJ (2000). Reliability and validity of DSM-IV axis V. *The American Journal of Psychiatry* **157**, 1858–1863.

Hua K, Zhang J, Wakana S, Jiang H, Li X, Reich DS, Calabresi PA, Pekar JJ, van Zijl PC, Mori S (2008). Tract probability maps in stereotaxic spaces: analyses of white matter anatomy and tract-specific quantification. *Neuroimage* **39**, 336–347.

Huang W, DiFranza JR, Kennedy DN, Zhang N, Ziedonis D, Ursprung S, King JA (2013). Progressive levels of physical dependence to tobacco coincide with changes in the anterior cingulum bundle microstructure. *PLoS ONE* **8**, e67837.

Hubl D, Koenig T, Strik W, Federspiel A, Kreis R, Boesch C, Maier SE, Schroth G, Lovblad K, Dierks T (2004). Pathways that make voices: white matter changes in auditory hallucinations. *Archives of General Psychiatry* **61**, 658–668.

Hudkins M, O'Neill J, Tobias MC, Bartzokis G, London ED (2012). Cigarette smoking and white matter microstructure. *Psychopharmacology* (*Berl*) **221**, 285–295.

Jacobsen LK, Picciotto MR, Heath CJ, Frost SJ, Tsou KA, Dwan RA, Jackowski MP, Constable RT, Mencl WE (2007). Prenatal and adolescent exposure to tobacco smoke modulates the development of white matter microstructure. *Journal of Neuroscience* **27**, 13491–13498.

James A, Hough M, James S, Winmill L, Burge L, Nijhawan S, Matthews PM, Zarei M. (2011). Greater white and grey matter changes associated with early cannabis use in adolescent-onset schizophrenia (AOS). *Schizophrenia Research* **128**, 91–97.

Jenkinson M, Beckmann CF, Behrens TE, Woolrich MW, Smith SM (2012). FSL. *Neuroimage* **62**, 782–790.

Karlsgodt KH, Niendam TA, Bearden CE, Cannon TD (2009). White matter integrity and prediction of social and role functioning in subjects at ultra-high risk for psychosis. *Biological Psychiatry* **66**, 562–569.

Katagiri N, Pantelis C, Nemoto T, Zalesky A, Hori M, Shimoji K, Saito J, Ito S, Dwyer DB, Fukunaga I, Morita K, Tsujino N, Yamaguchi T, Shiraga N, Aoki S, Mizuno M (2015). A longitudinal study investigating sub-threshold symptoms and white matter changes in individuals with an 'at risk mental state' (ARMS). *Schizophrenia Research* **162**, 7–13.

Kikinis Z, Makris N, Finn CT, Bouix S, Lucia D, Coleman MJ, Tworog-Dube E, Kikinis R, Kucherlapati R, Shenton ME, Kubicki M (2013). Genetic contributions to changes of fiber tracts of ventral visual stream in 22q11.2 deletion syndrome. *Brain Imaging and Behavior* **7**, 316–325.

Kim JH, Loy DN, Wang Q, Budde MD, Schmidt RE, Trinkaus K, Song SK (2010). Diffusion tensor imaging at 3

hours after traumatic spinal cord injury predicts long-term locomotor recovery. *Journal of Neurotrauma* **27**, 587–598.

Kindlmann G, Ennis DB, Whitaker RT, Westin CF (2007). Diffusion tensor analysis with invariant gradients and rotation tangents. *IEE Transactions on Medical Imaging* **26**, 1483–1499.

Konukoglu E, Coutu JP, Salat DH, Fischl B (2016). Multivariate statistical analysis of diffusion imaging parameters using partial least squares: application to white matter variations in Alzheimer's disease. *Neuroimage* **134**, 573–586.

Krishnan A, Williams LJ, McIntosh AR, Abdi H (2011). Partial Least Squares (PLS) methods for neuroimaging: a tutorial and review. *Neuroimage* **56**, 455–475.

Kumar J, Iwabuchi S, Oowise S, Balain V, Palaniyappan L, Liddle PF (2015). Shared white-matter dysconnectivity in schizophrenia and bipolar disorder with psychosis. *Psychological Medicine* **45**, 759–770.

Lane SD, Steinberg JL, Ma L, Hasan KM, Kramer LA, Zuniga EA, Narayana PA, Moeller FG (2010). Diffusion tensor imaging and decision making in cocaine dependence. *PLoS ONE* **5**, e11591.

Lee SH, Kubicki M, Asami T, Seidman LJ, Goldstein JM, Mesholam-Gately RI, McCarley RW, Shenton ME (2013). Extensive white matter abnormalities in patients with first-episode schizophrenia: a Diffusion Tensor Iimaging (DTI) study. *Schizophrenia Research* **143**, 231–238.

Li J, Li XY, Feng DF, Gu L (2011). Quantitative evaluation of microscopic injury with diffusion tensor imaging in a rat model of diffuse axonal injury. *European Journal of Neuroscience* **33**, 933–945.

Li Y, Xie S, Liu B, Song M, Chen Y, Li P, Lu L, Lv L, Wang H, Yan H, Yan J, Zhang H, Zhang D, Jiang T (2016). Diffusion magnetic resonance imaging study of schizophrenia in the context of abnormal neurodevelopment using multiple site data in a Chinese Han population. *Transl. Psychiatry* **6**, e715.

Liao Y, Tang J, Deng Q, Deng Y, Luo T, Wang X, Chen H, Liu T, Chen X, Brody AL, Hao W (2011). Bilateral fronto-parietal integrity in young chronic cigarette smokers: a diffusion tensor imaging study. *PLoS ONE* **6**, e26460.

Lim KO, Choi SJ, Pomara N, Wolkin A, Rotrosen JP (2002). Reduced frontal white matter integrity in cocaine dependence: a controlled diffusion tensor imaging study. *Biological Psychiatry* **51**, 890–895.

Lin F, Wu G, Zhu L, Lei H (2013). Heavy smokers show abnormal microstructural integrity in the anterior corpus callosum: a diffusion tensor imaging study with tract-based spatial statistics. *Drug and Alcohol Dependence* **129**, 82–87.

Ling J, Merideth F, Caprihan A, Pena A, Teshiba T, Mayer AR (2012). Head injury or head motion? Assessment and quantification of motion artifacts in diffusion tensor imaging studies. *Human Brain Mapping* **33**, 50–62.

Ma L, Hasan KM, Steinberg JL, Narayana PA, Lane SD, Zuniga EA, Kramer LA, Moeller FG (2009). Diffusion tensor imaging in cocaine dependence: regional effects of cocaine on corpus callosum and effect of cocaine administration route. *Drug and Alcohol Dependence* **104**, 262–267.

Mandl RC, Pasternak O, Cahn W, Kubicki M, Kahn RS, Shenton ME, Hulshoff Pol HE (2015). Comparing free water imaging and magnetization transfer measurements in schizophrenia. *Schizophrenia Research* **161**, 126–132.

McIntosh AR, Bookstein FL, Haxby JV, Grady CL (1996). Spatial pattern analysis of functional brain images using partial least squares. *Neuroimage* **3**, 143–157.

McIntosh AR, Lobaugh NJ (2004). Partial least squares analysis of neuroimaging data: applications and advances. *Neuroimage* **23**(Suppl. 1), S250–S263.

McLelland VC, Chan D, Ferber S, Barense MD (2014). Stimulus familiarity modulates functional connectivity of the perirhinal cortex and anterior hippocampus during visual discrimination of faces and objects. *Frontiers in Human Neuroscience* **8**, 117.

Meyer EC, Carrion RE, Cornblatt BA, Addington J, Cadenhead KS, Cannon TD, McGlashan TH, Perkins DO, Tsuang MT, Walker EF, Woods SW, Heinssen R, Seidman LJ (2014). The relationship of neurocognition and negative symptoms to social and role functioning over time in individuals at clinical high risk in the first phase of the North American Prodrome Longitudinal Study. *Schizophrenia Bulletin* **40**, 1452–1461.

Mittal VA, Dean DJ, Bernard JA, Orr JM, Pelletier-Baldelli A, Carol EE, Gupta T, Turner J, Leopold DR, Robustelli BL, Millman ZB (2014). Neurological soft signs predict abnormal cerebellar-thalamic tract development and negative symptoms in adolescents at high risk for psychosis: a longitudinal perspective. *Schizophrenia Bulletin* **40**, 1204–1215.

Moeller FG, Hasan KM, Steinberg JL, Kramer LA, Dougherty DM, Santos RM, Valdes I, Swann AC, Barratt ES, Narayana PA (2005). Reduced anterior corpus callosum white matter integrity is related to increased impulsivity and reduced discriminability in cocaine-dependent subjects: diffusion tensor imaging. *Neuropsychopharmacology* **30**, 610–617.

Mori S, van Zijl P (2007). Human white matter atlas. *The American Journal of Psychiatry* **164**, 1005.

Morrison AP, French P, Stewart SL, Birchwood M, Fowler D, Gumley AI, Jones PB, Bentall RP, Lewis SW, Murray GK, Patterson P, Brunet K, Conroy J, Parker S, Reilly T, Byrne R, Davies LM, Dunn G (2012). Early detection and intervention evaluation for people at risk of psychosis: multisite randomised controlled trial. *British Medical Journal* **344**, e2233.

Mulert C, Scarr E (2012). Editorial: new treatment strategies in schizophrenia beyond dopamine: glutamatergic neurotransmission and more. *Current Pharmaceutical Biotechnology* **13**, 1474–1475.

Narayana PA, Herrera JJ, Bockhorst KH, Esparza-Coss E, Xia Y, Steinberg JL, Moeller FG (2014). Chronic cocaine administration causes extensive white matter damage in brain: diffusion tensor imaging and immunohistochemistry studies. *Psychiatric Research* **221**, 220–230.

Nestor PG, O'Donnell BF, McCarley RW, Niznikiewicz M, Barnard J, Jen SZ, Bookstein FL, Shenton ME (2002). A new statistical method for testing hypotheses of neuropsychological/MRI relationships in schizophrenia: partial least squares analysis. *Schizophrenia Research* **53**, 57–66.

Nordholm D, Poulsen HE, Hjorthoj C, Randers L, Nielsen MO, Wulff S, Krakauer K, Norbak-Emig H, Henriksen T,

Glenthoj B, Nordentoft M (2016). Systemic oxidative DNA and RNA damage are not increased during early phases of psychosis: a case control study. *Psychiatry Research* **241**, 201–206.

Ohtani T, Bouix S, Lyall AE, Hosokawa T, Saito Y, Melonakos E, Westin CF, Seidman LJ, Goldstein J, Mesholam-Gately R, Petryshen T, Wojcik J, Kubicki M (2015). Abnormal white matter connections between medial frontal regions predict symptoms in patients with first episode schizophrenia. *Cortex* **71**, 264–276.

Oldfield RC (1971). The assessment and analysis of handedness: the Edinburgh inventory. *Neuropsychologia* **9**, 97–113.

Paul RH, Grieve SM, Niaura R, David SP, Laidlaw DH, Cohen R, Sweet L, Taylor G, Clark RC, Pogun S, Gordon E (2008). Chronic cigarette smoking and the microstructural integrity of white matter in healthy adults: a diffusion tensor imaging study. *Nicotine and Tobacco Research* **10**, 137–147.

Perez-Iglesias R, Tordesillas-Gutierrez D, Barker GJ, McGuire PK, Roiz-Santianez R, Mata I, de Lucas EM, Quintana F, Vazquez-Barquero JL, Crespo-Facorro B (2010). White matter defects in first episode psychosis patients: a voxelwise analysis of diffusion tensor imaging. *Neuroimage* **49**, 199–204.

Peters BD, de Haan L, Dekker N, Blaas J, Becker HE, Dingemans PM, Akkerman EM, Majoie CB, van Amelsvoort TA, den Heeten GJ, Linszen DH (2008). White matter fibertracking in first-episode schizophrenia, schizoaffective patients and subjects at ultra-high risk of psychosis. *Neuropsychobiology* **58**, 19–28.

Peters BD, Dingemans PM, Dekker N, Blaas J, Akkerman E, van Amelsvoort TA, Majoie CB, den Heeten GJ, Linszen DH, de Haan L (2010). White matter connectivity and psychosis in ultra-high-risk subjects: a diffusion tensor fiber tracking study. *Psychiatry Research* **181**, 44–50.

Peters BD, Schmitz N, Dingemans PM, van Amelsvoort TA, Linszen DH, de Haan L, Majoie CB, den Heeten GJ (2009). Preliminary evidence for reduced frontal white matter integrity in subjects at ultra-high-risk for psychosis. *Schizophrenia Research* **111**, 192–193.

Pettersson-Yeo W, Benetti S, Marquand AF, Dell'acqua F, Williams SC, Allen P, Prata D, McGuire P, Mechelli A (2013). Using genetic, cognitive and multi-modal neuroimaging data to identify ultra-high-risk and first-episode psychosis at the individual level. *Psychological Medicine* **43**, 2547–2562.

Protzner AB, Hargreaves IS, Campbell JA, Myers-Stewart K, van Sophia H, Goodyear BG, Sargious P, Pexman PM (2016). This is your brain on Scrabble: neural correlates of visual word recognition in competitive Scrabble players as measured during task and resting-state. *Cortex* **75**, 204–219.

Reese TG, Heid O, Weisskoff RM, Wedeen VJ (2003). Reduction of eddy-current-induced distortion in diffusion MRI using a twice-refocused spin echo. *Magnetic Resonance in Medicine* **49**, 177–182.

Rigucci S, Santi G, Corigliano V, Imola A, Rossi-Espagnet C, Mancinelli I, De Pisa E, Manfredi G, Bozzao A, Carducci F, Girardi P, Comparelli A (2016). White matter microstructure in ultra-high risk and first episode schizophrenia: a prospective study. *Psychiatry Research* **247**, 42–48.

Roalf DR, Quarmley M, Elliott MA, Satterthwaite TD, Vandekar SN, Ruparel K, Gennatas ED, Calkins ME, Moore TM, Hopson R, Prabhakaran K, Jackson CT, Verma R, Hakonarson H, Gur RC, Gur RE (2016). The impact of quality assurance assessment on diffusion tensor imaging outcomes in a large-scale population-based cohort. *Neuroimage* **125**, 903–919.

Savjani RR, Velasquez KM, Thompson-Lake DG, Baldwin PR, Eagleman DM, De La Garza R, Salas R (2014). Characterizing white matter changes in cigarette smokers via diffusion tensor imaging. *Drug and Alcohol Dependence* **145**, 134–142.

Schlosser DA, Campellone TR, Biagianti B, Delucchi KL, Gard DE, Fulford D, Stuart BK, Fisher M, Loewy RL, Vinogradov S (2015). Modeling the role of negative symptoms in determining social functioning in individuals at clinical high risk of psychosis. *Schizophrenia Research* **169**, 204–208.

Schmidt A, Lenz C, Smieskova R, Harrisberger F, Walter A, Riecher-Rossler A, Simon A, Lang UE, McGuire P, Fusar-Poli P, Borgwardt SJ (2015). Brain diffusion changes in emerging psychosis and the impact of state-dependent psychopathology. *Neurosignals* **23**, 71–83.

Seitz J, Zuo JX, Lyall AE, Makris N, Kikinis Z, Bouix S, Pasternak O, Fredman E, Duskin J, Goldstein JM, Petryshen TL, Mesholam-Gately RI, Wojcik J, McCarley RW, Seidman LJ, Shenton ME, Koerte IK, Kubicki M (2016). Tractography analysis of 5 white matter bundles and their clinical and cognitive correlates in early-course schizophrenia. *Schizophrenia Bulletin* **42**, 762–771.

Seok JH, Park HJ, Chun JW, Lee SK, Cho HS, Kwon JS, Kim JJ (2007). White matter abnormalities associated with auditory hallucinations in schizophrenia: a combined study of voxel-based analyses of diffusion tensor imaging and structural magnetic resonance imaging. *Psychiatry Research* **156**, 93–104.

Shergill SS, Kanaan RA, Chitnis XA, O'Daly O, Jones DK, Frangou S, Williams SC, Howard RJ, Barker GJ, Murray RM, McGuire P (2007). A diffusion tensor imaging study of fasciculi in schizophrenia. *The American Journal of Psychiatry* **164**, 467–473.

Shin YW, Kwon JS, Ha TH, Park HJ, Kim DJ, Hong SB, Moon WJ, Lee JM, Kim IY, Kim SI, Chung EC (2006). Increased water diffusivity in the frontal and temporal cortices of schizophrenic patients. *Neuroimage* **30**, 1285–1291.

Skelly LR, Calhoun V, Meda SA, Kim J, Mathalon DH, Pearlson GD (2008). Diffusion tensor imaging in schizophrenia: relationship to symptoms. *Schizophrenia Research* **98**, 157–162.

Smith SM (2002). Fast robust automated brain extraction. *Human Brain Mapping* **17**, 143–155.

Smith SM, Jenkinson M, Johansen-Berg H, Rueckert D, Nichols TE, Mackay CE, Watkins KE, Ciccarelli O, Cader MZ, Matthews PM, Behrens TE (2006). Tract-based spatial

statistics: voxelwise analysis of multi-subject diffusion data. *Neuroimage* **31**, 1487–1505.

Smith SM, Jenkinson M, Woolrich MW, Beckmann CF, Behrens TE, Johansen-Berg H, Bannister PR, De Luca M, Drobnjak I, Flitney DE, Niazy RK, Saunders J, Vickers J, Zhang Y, De Stefano N, Brady JM, Matthews PM (2004). Advances in functional and structural MR image analysis and implementation as FSL. *Neuroimage* **23**(Suppl. 1), S208–S219.

Smith SM, Nichols TE (2009). Threshold-free cluster enhancement: addressing problems of smoothing, threshold dependence and localisation in cluster inference. *Neuroimage* **44**, 83–98.

Song SK, Sun SW, Ramsbottom MJ, Chang C, Russell J, Cross AH (2002). Dysmyelination revealed through MRI as increased radial (but unchanged axial) diffusion of water. *Neuroimage* **17**, 1429–1436.

Song SK, Yoshino J, Le TQ, Lin SJ, Sun SW, Cross AH, Armstrong RC (2005). Demyelination increases radial diffusivity in corpus callosum of mouse brain. *Neuroimage* **26**, 132–140.

Spalletta G, De Rossi P, Piras F, Iorio M, Dacquino C, Scanu F, Girardi P, Caltagirone C, Kirkpatrick B, Chiapponi C (2015). Brain white matter microstructure in deficit and non-deficit subtypes of schizophrenia. *Psychiatry Research* **231**, 252–261.

Sun H, Lui S, Yao L, Deng W, Xiao Y, Zhang W, Huang X, Hu J, Bi F, Li T, Sweeney JA, Gong Q (2015). Two patterns of white matter abnormalities in medication-naive patients with first-episode schizophrenia revealed by diffusion tensor imaging and cluster analysis. *JAMA Psychiatry* **72**, 678–686.

Sun SW, Liang HF, Le TQ, Armstrong RC, Cross AH, Song SK (2006*a*). Differential sensitivity of *in vivo* and *ex vivo* diffusion tensor imaging to evolving optic nerve injury in mice with retinal ischemia. *Neuroimage* **32**, 1195–1204.

Sun SW, Liang HF, Trinkaus K, Cross AH, Armstrong RC, Song SK (2006*b*). Noninvasive detection of cuprizone induced axonal damage and demyelination in the mouse corpus callosum. *Magnetic Resonance in Medicine* **55**, 302–308.

Szeszko PR, Robinson DG, Ashtari M, Vogel J, Betensky J, Sevy S, Ardekani BA, Lencz T, Malhotra AK, McCormack J, Miller R, Lim KO, Gunduz-Bruce H, Kane JM, Bilder RM (2008). Clinical and neuropsychological correlates of white matter abnormalities in recent onset schizophrenia. *Neuropsychopharmacology* **33**, 976–984.

Tyszka JM, Readhead C, Bearer EL, Pautler RG, Jacobs RE (2006). Statistical diffusion tensor histology reveals regional dysmyelination effects in the shiverer mouse mutant. *Neuroimage* **29**, 1058–1065.

Umene-Nakano W, Yoshimura R, Kakeda S, Watanabe K, Hayashi K, Nishimura J, Takahashi H, Moriya J, Ide S, Ueda I, Hori H, Ikenouchi-Sugita A, Katsuki A, Atake K, Abe O, Korogi Y, Nakamura J (2014). Abnormal white matter integrity in the corpus callosum among smokers: tract-based spatial statistics. *PLoS ONE* **9**, e87890.

van Dellen E, Bohlken MM, Draaisma L, Tewarie PK, van Lutterveld R, Mandl R, Stam CJ, Sommer IE (2016). Structural brain network disturbances in the psychosis spectrum. *Schizophrenia Bulletin* **42**, 782–789.

van Ewijk H, Groenman AP, Zwiers MP, Heslenfeld DJ, Faraone SV, Hartman CA, Luman M, Greven CU, Hoekstra PJ, Franke B, Buitelaar J, Oosterlaan J (2015). Smoking and the developing brain: altered white matter microstructure in attention-deficit/hyperactivity disorder and healthy controls. *Human Brain Mapping* **36**, 1180–1189.

Viswanath H, Velasquez KM, Thompson-Lake DG, Savjani R, Carter AQ, Eagleman D, Baldwin PR, De La Garza R, Salas R (2015). Alterations in interhemispheric functional and anatomical connectivity are associated with tobacco smoking in humans. *Frontiers in Human Neuroscience* **9**, 116.

von Hohenberg CC, Pasternak O, Kubicki M, Ballinger T, Vu MA, Swisher T, Green K, Giwerc M, Dahlben B, Goldstein JM, Woo TU, Petryshen TL, Mesholam-Gately RI, Woodberry KA, Thermenos HW, Mulert C, McCarley RW, Seidman LJ, Shenton ME (2014). White matter microstructure in individuals at clinical high risk of psychosis: a whole-brain diffusion tensor imaging study. *Schizophrenia Bulletin* **40**, 895–903.

Wakana S, Caprihan A, Panzenboeck MM, Fallon JH, Perry M, Gollub RL, Hua K, Zhang J, Jiang H, Dubey P, Blitz A, van Zijl P, Mori S (2007). Reproducibility of quantitative tractography methods applied to cerebral white matter. *Neuroimage* **36**, 630–644.

Wang C, Ji F, Hong Z, Poh JS, Krishnan R, Lee J, Rekhi G, Keefe RS, Adcock RA, Wood SJ, Fornito A, Pasternak O, Chee MW, Zhou J (2016). Disrupted salience network functional connectivity and white-matter microstructure in persons at risk for psychosis: findings from the LYRIKS study. *Psychological Medicine* **46**, 2771–2783.

Wechsler D (1997). *Administration and Scoring Manual for the Wechsler Adult Intelligence Scale–3rd Revision (WAIS-III)*, Psychological Corporation: San Antonio.

Whitford TJ, Kubicki M, Schneiderman JS, O'Donnell LJ, King R, Alvarado JL, Khan U, Markant D, Nestor PG, Niznikiewicz M, McCarley RW, Westin CF, Shenton ME (2010). Corpus callosum abnormalities and their association with psychotic symptoms in patients with schizophrenia. *Biological Psychiatry* **68**, 70–77.

Wigand M, Kubicki M, Clemm von HC, Leicht G, Karch S, Eckbo R, Pelavin PE, Hawley K, Rujescu D, Bouix S, Shenton ME, Mulert C (2015). Auditory verbal hallucinations and the interhemispheric auditory pathway in chronic schizophrenia. *The World Journal of Biological Psychiatry* **16**, 31–44.

Wing JK, Babor T, Brugha T, Burke J, Cooper JE, Giel R, Jablenski A, Regier D, Sartorius N (1990). SCAN. Schedules for clinical assessment in neuropsychiatry. *Archives of General Psychiatry* **47**, 589–593.

Wolkin A, Choi SJ, Szilagyi S, Sanfilipo M, Rotrosen JP, Lim KO (2003). Inferior frontal white matter anisotropy and negative symptoms of schizophrenia: a diffusion tensor imaging study. *The American Journal of Psychiatry* **160**, 572–574.

Woolrich MW, Jbabdi S, Patenaude B, Chappell M, Makni S, Behrens T, Beckmann C, Jenkinson M, Smith SM (2009). Bayesian analysis of neuroimaging data in FSL. *Neuroimage* **45**, S173–S186.

Xie M, Tobin JE, Budde MD, Chen CI, Trinkaus K, Cross AH, McDaniel DP, Song SK, Armstrong RC (2010). Rostrocaudal analysis of corpus callosum demyelination and axon damage across disease stages refines diffusion tensor imaging correlations with pathological features. *Journal of Neuropathology and Experimental Neurology* **69**, 704–716.

Yendiki A, Koldewyn K, Kakunoori S, Kanwisher N, Fischl B (2014). Spurious group differences due to head motion in a diffusion MRI study. *Neuroimage* **88**, 79–90.

Yu D, Yuan K, Zhang B, Liu J, Dong M, Jin C, Luo L, Zhai J, Zhao L, Zhao Y, Gu Y, Xue T, Liu X, Lu X, Qin W, Tian J (2016). White matter integrity in young smokers: a tract-based spatial statistics study. *Addiction Biology* **21**, 679–687.

Yucel M, Zalesky A, Takagi MJ, Bora E, Fornito A, Ditchfield M, Egan GF, Pantelis C, Lubman DI (2010). White-matter abnormalities in adolescents with long-term inhalant and cannabis use: a diffusion magnetic resonance imaging study. *Journal of Psychiatry & Neuroscience* **35**, 409–412.

Yung AR, Phillips LJ, Yuen HP, Francey SM, McFarlane CA, Hallgren M, McGorry PD (2003). Psychosis prediction: 12-month follow up of a high-risk ("prodromal") group. *Schizophrenia Research* **60**, 21–32.

Yung AR, Yuen HP, McGorry PD, Phillips LJ, Kelly D, Dell'Olio M, Francey SM, Cosgrave EM, Killackey E, Stanford C, Godfrey K, Buckby J (2005). Mapping the onset of psychosis: the comprehensive assessment of at-risk mental states. *Australian & New Zealand Journal of Psychiatry* **39**, 964–971.

Zalesky A, Solowij N, Yucel M, Lubman DI, Takagi M, Harding IH, Lorenzetti V, Wang R, Searle K, Pantelis C, Seal M (2012). Effect of long-term cannabis use on axonal fibre connectivity. *Brain* **135**, 2245–2255.

Zeng B, Ardekani BA, Tang Y, Zhang T, Zhao S, Cui H, Fan X, Zhuo K, Li C, Xu Y, Goff DC, Wang J (2016). Abnormal white matter microstructure in drug-naive first episode schizophrenia patients before and after eight weeks of antipsychotic treatment. *Schizophrenia Research* **172**, 1–8.

Zhang XY, Fan FM, Chen DC, Tan YL, Tan SP, Hu K, Salas R, Kosten TR, Zunta-Soares G, Soares JC (2016). Extensive white matter abnormalities and clinical symptoms in drug-naive patients with first-episode schizophrenia: a voxel-based diffusion tensor imaging study. *Journal of Clinical Psychiatry* **77**, 205–211.

Zhu J, Zhuo C, Qin W, Wang D, Ma X, Zhou Y, Yu C (2015). Performances of diffusion kurtosis imaging and diffusion tensor imaging in detecting white matter abnormality in schizophrenia. *Neuroimage: Clinical* **7**, 170–176.

Ziegler G, Dahnke R, Winkler AD, Gaser C (2013). Partial least squares correlation of multivariate cognitive abilities and local brain structure in children and adolescents. *Neuroimage* **82**, 284–294.

https://doi.org/10.1017/S0033291717001210 Published online by Cambridge University Press